A Novel Design Method of Multi-Compartment Soma-Dendrite-Spine Model having Nonlinear Asynchronous CA Dynamics and its Applications to STDP-based Learning and FPGA Implementation

Masato Ishikawa
Faculty of Science and Engineering
Hosei University
Koganei, Tokyo, Japan
email masato.ishikawa.2h@stu.hosei.ac.jp

Hiroyuki Torikai
Faculty of Science and Engineering
Hosei University
Koganei, Tokyo, Japan
email torikai@hosei.ac.jp

***Abstract*—This paper designs a multi-compartment soma-dendrite-spine model having nonlinear dynamics of an asynchronous cellular automaton. The model can exhibit various propagations of action potentials observed in neurons and these propagations are analyzed in detailed. Then, using the analysis results, a novel systematic design method of the model is proposed. It is shown that the model designed by the proposed method can realize robust conditioning based on spike-timing dependent plasticity (STDP). Also, the designed model is implemented by a field programmable gate array (FPGA) and experiments validate its STDP-based conditioning function. It is then shown that the designed model consumes fewer hardware resources and lower power compared to an ODE-based multi-compartment model.**

***Index Terms*—Multi-Compartment Neuron Model, Asynchronous Cellular Automaton, Nonlinear Dynamics, STDP, Pavlovian Conditioning, FPGA, VLSI**

I. Introduction

A neuron typically consists of a soma, dendrites, spines, and axons, where the dendrite sometimes has complicated physical structure such as the one in Fig. 1(a) [1]. A wide variety of dendritic phenomena have been observed [2]-[8] such as forward and backward propagations of action potentials and their combinations. It has been suggested such various dendritic phenomena play important roles in neural information processing and *spike-timing dependent plasticity* (STDP) [9], where various STDP models have been also investigated in recent years [10]-[12]. One of the major modeling methods of the neuron reflecting its physical structure is a multi-compartment modeling method as shown in Fig. 1(b) [9]-[14], where the dynamics of the neuron is modeled by a coupled system of small compartments.

Concerning mathematical modeling and VLSI implementation methods of neural systems, there exist four approaches depending on continuousness of time and state as follows [15]. The first approach is to model a neural system by a nonlinear ordinary differential equation, which has a continuous time and continuous states. Such a model can be implemented by a nonlinear electronic circuit. The second approach is to model a neural system by a nonlinear difference equation, which has a discrete time and continuous states. Such a model can be implemented by a switched capacitor circuit. The third approach is to model a neural system by a numerical integration in a fixed-point or a floating-point number format or by a cellular automaton, which have discrete times and discrete states. Such models can be implemented by digital processors or sequential logics. The fourth approach is to model a neural system by an asynchronous cellular automaton, which has a continuous (state transition) time and discrete states. Such a model can be implemented by an asynchronous sequential logic. Most conventional neural systems are modeled and implemented based on the first, the second, or the third approach [16]. On the other hand, our group and some other groups have designed neural system models based on the fourth approach [13]-[15][17]-[20] and have shown such neural system models

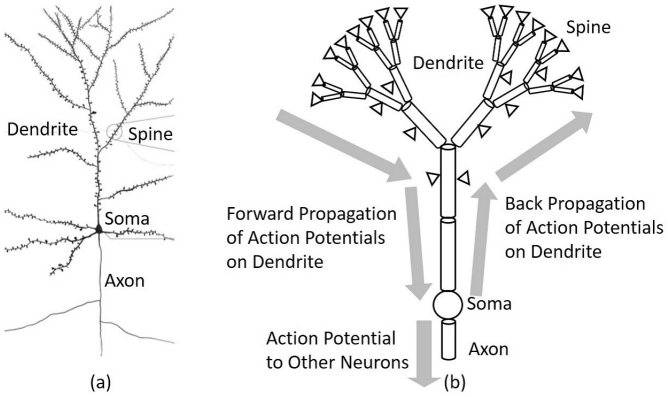

Fig. 1. (a) Anatomical structure of neuron [1]. (b) Multi-compartment soma-dendrite-spine model [9]-[14]. Forward propagations of action potentials (from dendrite to soma) and backward propagations of action potentials (from soma to dendrite and from dendrite to dendrite) play important roles in conditioning of the model based on *spike timing dependent plasticity* (STDP) in a spine.

This work was partially supported by the KAKENHI Grant-in-Aid for Scientific Research Grant Number 18K11482.

978-1-7281-6926-2/20/$31.00 ©2020 IEEE

consume much fewer hardware resources compared to the digital processor approach [13][15][17]-[19]. In these researches, multi-compartment soma-dendrite-spine models designed by the fourth approach are also designed [13][14]. However, the following important questions are still unclear.

- how to design the multi-compartment soma-dendrite-spine model having the nonlinear dynamics of the asynchronous cellular automaton so that it can exhibit various dendritic phenomena observed in neurons;
- how to design the model so that it can realize robust conditioning or learning; and
- how to design the model so that it consumes few hardware resources and low power.

In this paper, some clear answers to these questions are provided. The main results of this paper and their novelties and significances include the following points.

- This paper provides detailed analysis results of various propagations of action potentials in the multi-compartment soma-dendrite-spine model having the nonlinear dynamics of the asynchronous cellular automaton for the first time.
- The above analysis results can be used as powerful tools to design the model. Actually, this paper proposes a novel systematic design method of the model so that it can realize robust Pavlovian conditioning [21] based on the STDP, where the analysis results play central roles in the proposed design method.
- It is shown that the model designed by the proposed method consumes fewer hardware resources and lower power compared to an *ordinary differential equation* (ODE) multi-compartment neuron model.
- The above results suggest that this paper will contribute to design biologically plausible neural network hardware suitable for neural prosthetic devices [22] such as a "*biologically plausible, small, low power, and robustly learnable brain implant chip.*"

II. Multi-compartment soma-dendrite-spine model

A. Structure of multi-compartment soma-dendrite-spine model

In this paper, the multi-compartment soma-dendrite-spine model in Fig. 2 is designed and analyzed. Major features of the structure of the model are as follows.

- The multi-compartment soma-dendrite-spine model have Q membrane units $\{\mathcal{M}_0, \mathcal{M}_1, \cdots, \mathcal{M}_{Q-1}\}$, where all the membrane units are assumed to be connected, i.e., there is no isolated membrane unit. In the case of Fig. 2, the number Q of the membrane unit is 6.
- The 0-th membrane unit $\mathcal{M}_0$ is used as a soma compartment. The other membrane units $\{\mathcal{M}_1, \cdots, \mathcal{M}_{Q-1}\}$ are used as dendrite compartments and form a dendritic tree structure.
- A spine unit $\mathcal{S}_i$ can be connected to the membrane unit $\mathcal{M}_i$ (not necessarily). In the case of Fig. 2, the spine units $\mathcal{S}_4$ and $\mathcal{S}_5$ are connected to the membrane units $\mathcal{M}_4$ and $\mathcal{M}_5$, respectively.

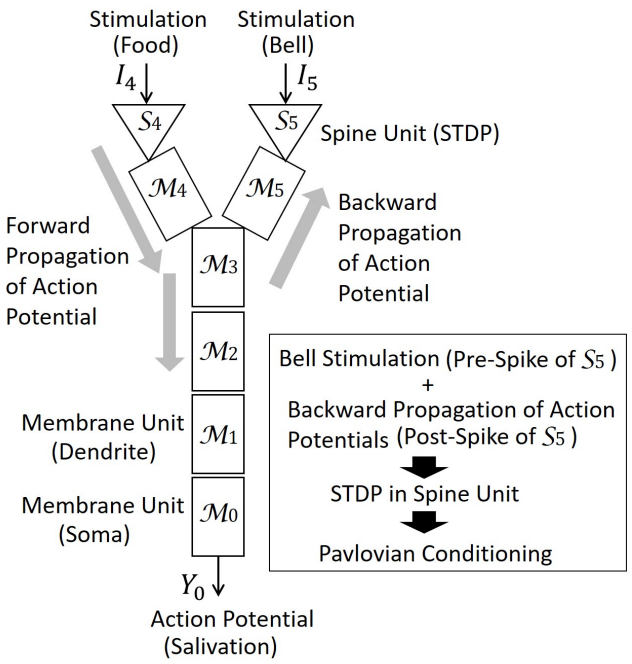

Fig. 2. Whole structure of the multi-compartment soma-dendrite-spine model designed in this paper and roles of propagations of action potentials in STDP-based Pavlovian conditioning.

The multi-compartment model can exhibit a wide variety of propagations of action potentials in response to stimulations. This paper studies how such various propagations of action potentials can realize the Pavlovian conditioning in the multi-compartment model as follows (see also Fig. 2).

- The stimulation I_4 to the spine unit $\mathcal{S}_4$ corresponds to giving a "food" to the model.
- The stimulation I_5 to the spine unit $\mathcal{S}_5$ corresponds to ringing a "bell" in front of the model.
- The action potential Y_0 of the soma compartment $\mathcal{M}_0$ corresponds to "salivation" of the model.
- The stimulations I_4 and I_5 and the salivation Y_0 cause various propagations of action potentials in the multi-compartment model such as forward and backward propagations of action potentials and their combinations.
- The spine unit $\mathcal{S}_5$ exhibits *spike timing dependent plasticity* (STDP) in response to bell stimulations I_5 (corresponding to pre-synaptic spikes) and backward propagations of action potentials Y_5 (corresponding to post-synaptic spikes) from the dendrite compartment $\mathcal{M}_5$.
- Due to the STDP, the multi-compartment model is conditioned so that it salivates in response to the bell stimulation I_5 without giving the food stimulation I_4.

B. Asynchronous discrete dynamics of membrane unit

In Fig. 3, a circuit diagram of the membrane unit $\mathcal{M}_i$ is shown. Each i-th membrane unit $\mathcal{M}_i$ has two registers storing the following two discrete states.

Discrete membrane potential

$$V_i \in \{0, 1, \cdots, M-1\} = \boldsymbol{M},$$

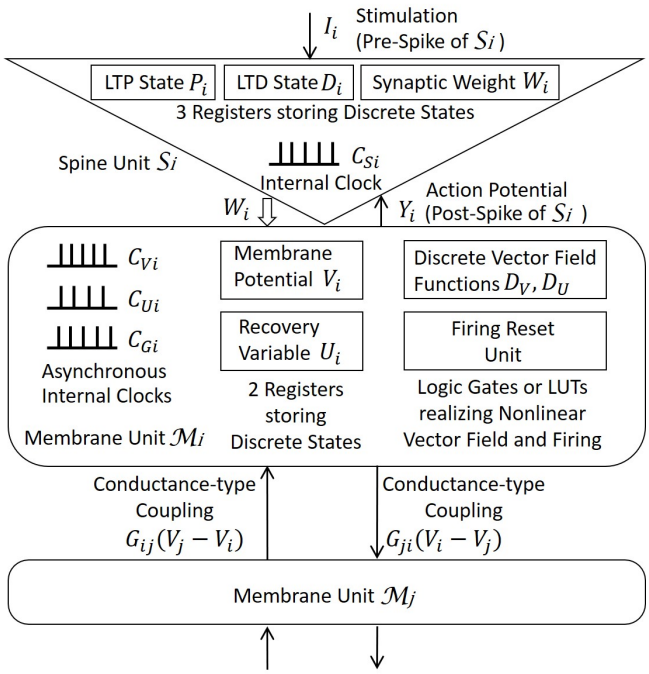

Fig. 3. Circuit diagrams of the membrane unit $\mathcal{M}_i$ and the spine unit $\mathcal{S}_i$.

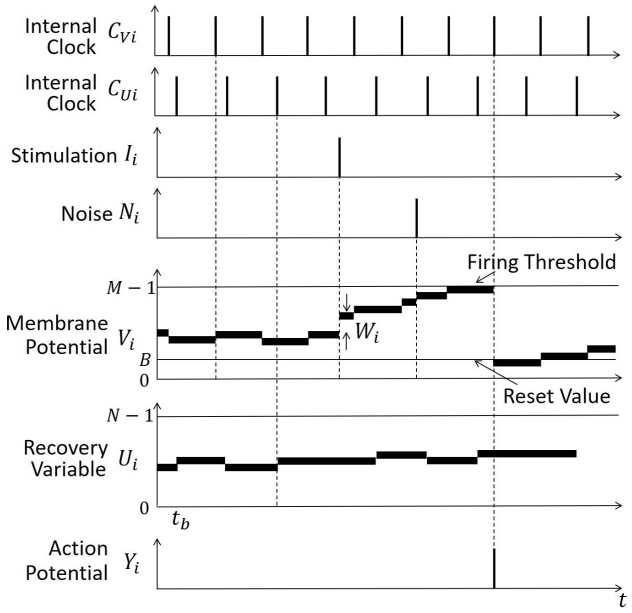

Fig. 4. Typical asynchronous transitions of the discrete states of the membrane unit $\mathcal{M}_i$. The internal clocks C_{Vi} and C_{Ui} are assumed to be periodic, to have different periods, and to be asynchronous.

Discrete recovery variable

$$U_i \in \{0, 1, \cdots, N-1\} = \boldsymbol{N},$$

where the integer parameters $M > 0$ and $N > 0$ determine the resolutions of the discrete membrane potential V_i and the discrete recovery variable U_i, respectively. Also, as shown in Fig. 3, each i-th membrane unit $\mathcal{M}_i$ has the following asynchronous internal clocks.

Asynchronous internal clocks for vector field

$$C_{Vi}(t) = \begin{cases} 1 & \text{if } t \in \{t_{Vi}^{(1)}, t_{Vi}^{(2)}, \cdots\}, \\ 0 & \text{otherwise,} \end{cases}$$

$$C_{Ui}(t) = \begin{cases} 1 & \text{if } t \in \{t_{Ui}^{(1)}, t_{Ui}^{(2)}, \cdots\}, \\ 0 & \text{otherwise,} \end{cases}$$

where $t_{Vi}^{(n)}$ and $t_{Ui}^{(n)}$ represent spike timings (or rising edges) of the clocks. As shown in Fig. 4, the internal clocks C_{Vi} and C_{Ui} are assumed to be periodic, to have different periods, and to be asynchronous. As shown in Fig. 4, the internal clocks C_{Vi} and C_{Ui} trigger the following asynchronous transitions of the discrete states V_i and U_i of the membrane unit $\mathcal{M}_i$.

Asynchronous state transitions by clocks C_{Vi} and C_{Ui}

$$\begin{aligned} V_i(t^+) &= V_i(t) + D_V(V_i, U_i) \ \text{ if } \ C_{Vi}(t) = 1, \\ U_i(t^+) &= U_i(t) + D_U(V_i, U_i) \ \text{ if } \ C_{Ui}(t) = 1, \end{aligned} \tag{1}$$

where $D_V(V_i, U_i) : \boldsymbol{M} \times \boldsymbol{N} \to \{-1, 0, 1\}$ and $D_U(V_i, U_i) : \boldsymbol{M} \times \boldsymbol{N} \to \{-1, 0, 1\}$ are discrete functions defined by

$$\begin{aligned} &D_V(V_i, U_i) = 1 \quad \text{if } (V_i, U_i) \in \mathbf{S}_i^{++} \cup \mathbf{S}_i^{+-}, \\ &D_V(V_i, U_i) = -1 \quad \text{if } (V_i, U_i) \in \mathbf{S}_i^{-+} \cup \mathbf{S}_i^{--}, \\ &D_V(V_i, U_i) = 0 \quad \text{if } (V_i, U_i) \in \mathbf{S}_i^{0}, \\ &D_U(V_i, U_i) = 1 \quad \text{if } (V_i, U_i) \in \mathbf{S}_i^{++} \cup \mathbf{S}_i^{-+}, \\ &D_U(V_i, U_i) = -1 \quad \text{if } (V_i, U_i) \in \mathbf{S}_i^{+-} \cup \mathbf{S}_i^{--}, \\ &D_U(V_i, U_i) = 0 \quad \text{if } (V_i, U_i) \in \mathbf{S}_i^{0}, \end{aligned}$$

$$\begin{aligned} &\mathbf{S}_i^{++} \equiv \{(V_i, U_i) | U_i < f_V(V_i), U_i \le f_U(V_i)\}, \\ &\mathbf{S}_i^{-+} \equiv \{(V_i, U_i) | U_i \ge f_V(V_i), U_i < f_U(V_i)\}, \\ &\mathbf{S}_i^{+-} \equiv \{(V_i, U_i) | U_i \le f_V(V_i), U_i > f_U(V_i)\}, \\ &\mathbf{S}_i^{--} \equiv \{(V_i, U_i) | U_i > f_V(V_i), U_i \ge f_U(V_i)\}, \\ &\mathbf{S}_i^{0} \equiv \{(V_i, U_i) | (V_i, U_i) \notin \mathbf{S}_i^{++} \cup \mathbf{S}_i^{+-} \cup \mathbf{S}_i^{-+} \cup \mathbf{S}_i^{--}\}, \end{aligned}$$

where f_V and f_U are discrete functions defined by

$$\begin{aligned} &f_V(V_i) = \gamma(\lfloor k_1(V_i)^2 + k_2 V_i + k_3 \rfloor), \\ &f_U(V_i) = \gamma(\lfloor k_4 V_i + k_5 \rfloor), \\ &k_1 = \tfrac{f_1 M}{N^2}, \ k_2 = -2k_1 \lfloor f_2 N \rfloor, \\ &k_3 = k_1(\lfloor f_2 N \rfloor)^2 + \lfloor f_3 M \rfloor, \ k_4 = \tfrac{f_4 M}{N}, \ k_5 = \lfloor f_5 M \rfloor, \end{aligned}$$

where $\lfloor \cdot \rfloor$ is the floor function, $\gamma(x) = x$ for $-1 \le x \le M$, and $\gamma(x) = -1$ for $x < -1$. Note that the discrete membrane potential V_i (the discrete recovery variable U_i) is assumed to be saturated at 0 and $M-1$ (0 and $N-1$) and to exist in its range $\boldsymbol{M}$ (range $\boldsymbol{N}$) throughout the paper. The function D_V and D_U determine a nonlinear vector field of the membrane unit $\mathcal{M}_i$ and thus are called discrete vector field functions. As shown in Fig. 3, the discrete vector field functions D_V and D_U are implemented by logic gates or look-up-tables. As shown in Fig. 3, the spine unit $\mathcal{S}_i$ has a register storing the following synaptic weight.

Discrete synaptic weight

$$W_i \in \{0, 1, \cdots, W_{max}\},$$

where the integer parameter $W_{max} > 0$ determines the resolution of the discrete synaptic weight W_i. As shown in Figs. 2 and 3, the spine unit $\mathcal{S}_i$ accepts the following stimulation.

Stimulation

$$I_i(t) = \begin{cases} 1 & \text{if } t \in \{t_{Ii}^{(1)}, t_{Ii}^{(2)}, \cdots\}, \\ 0 & \text{otherwise,} \end{cases}$$

where $t_{Ii}^{(n)}$ represents spike timing (or rising edge) of the stimulation I_i. As shown in Fig. 4, the stimulation I_i to the spine unit $\mathcal{S}_i$ triggers the following transition of the discrete state V_i of the membrane unit $\mathcal{M}_i$.

Asynchronous state transition by stimulation I_i

$$V_i(t^+) = V_i(t) + W_i \ \text{ if } \ I_i(t) = 1. \tag{2}$$

The membrane unit $\mathcal{M}_i$ also accepts a noise

Noise

$$N_i(t) = \begin{cases} 1 & \text{if } t \in \{t_{Ni}^{(1)}, t_{Ni}^{(2)}, \cdots\}, \\ 0 & \text{otherwise,} \end{cases}$$

where $t_{Ni}^{(n)}$ represents spike timing (or rising edge) of the noise N_i. As shown in Fig. 4, the noise N_i triggers the following transition of the discrete state V_i of the membrane unit $\mathcal{M}_i$.

Asynchronous state transition by noise N_i

$$V_i(t^+) = V_i(t) + 1 \ \text{ if } \ N_i(t) = 1. \tag{3}$$

As shown in Fig. 4, the membrane unit $\mathcal{M}_i$ exhibits the following firing reset and generation of an action potential.

Firing reset

$$V_i(t^+) = B \ \text{ if } \ V_i(t) = M-1 \ \text{ and } \ C_{Vi}(t) = 1, \tag{4}$$

Action potential

$$Y_i(t) = \begin{cases} 1 & \text{if } \ V_i(t) = M-1 \ \text{ and } \ C_{Vi}(t) = 1, \\ 0 & \text{otherwise,} \end{cases} \tag{5}$$

where $B \in \boldsymbol{M}$ is the value to which the membrane potential V_i is reset. In this paper the parameter values of each membrane unit $\mathcal{M}_i$ are fixed to $(M, N, f_1, f_2, f_3, f_4, f_5, B) = (64, 64, 3.5, 0.45, -0.05, 1.5, -0.43, 10)$ in order to realize various dendritic phenomena.

C. Asynchronous discrete coupling of membrane units

As shown in Fig. 3, each i-th membrane unit $\mathcal{M}_i$ has the following internal clock.

Asynchronous internal clock for coupling

$$C_{Gi}(t) = \begin{cases} 1 & \text{if } t \in \{t_{Gi}^{(1)}, t_{Gi}^{(2)}, \cdots\}, \\ 0 & \text{otherwise,} \end{cases}$$

where $t_{Gi}^{(n)}$ represents spike timing (or rising edge) of the clock. In this paper, the internal clock C_{Gi} is assumed to be periodic as shown in Fig. 5, to have different periods from the internal clocks C_{Vi} and C_{Ui}, and to be asynchronous with C_{Vi} and C_{Ui}. Now, as shown in Fig. 3, let us assume the membrane units $\mathcal{M}_i$ and $\mathcal{M}_j$ are coupled. Then, as shown in Fig. 5, the internal clock C_{Gi} triggers the following transition of the discrete state V_i of the membrane unit $\mathcal{M}_i$.

Asynchronous coupling by clock C_{Gi}

$$V_i(t^+) = V_i(t) + G_{ij}(V_j - V_i) \ \text{ if } \ C_{Gi}(t) = 1, \tag{6}$$

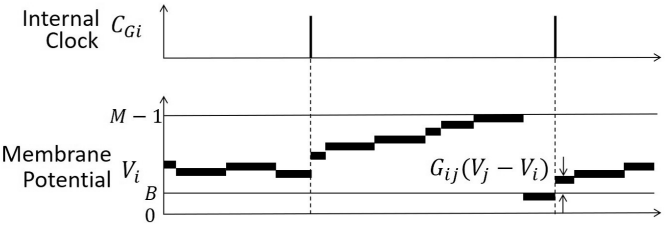

Fig. 5. Asynchronous discrete coupling of membrane units $\mathcal{M}_i$ and $\mathcal{M}_j$.

where $G_{ij} : \{-(M-1), \cdots, -1, 0, 1, \cdots, M-1\} \to \{-(M-1), \cdots, -1, 0, 1, \cdots, M-1\}$ is a discrete function defined by

$$G_{ij}(V) = \begin{cases} \lfloor g_{ij} V \rfloor & \text{if } -T_{ij} \le V \le T_{ij}, \\ 0 & \text{otherwise,} \end{cases}$$

where $T_{ij} \in \boldsymbol{M}$ and $g_{ij} \in \boldsymbol{R}$ are parameters determining the nonlinearity of the coupling. In this paper, we assume $g_{01} = \alpha/2$, $g_{12} = g_{23} = g_{35} = g_{34} = \alpha$, $g_{56} = 0.3$, $g_{21} = g_{32} = g_{43} = g_{53} = \beta$, $T_{01} = T_{12} = T_{21} = T_{23} = T_{32} = T_{34} = T_{43} = T_{35} = T_{53} = 30$, and $T_{10} = M-1$.

D. Asynchronous discrete STDP of spine unit

As shown in Fig. 2, a spine unit $\mathcal{S}_i$ can be connected to the membrane unit $\mathcal{M}_i$ (not necessarily). Now, as shown in Fig. 3, let us assume the spine unit $\mathcal{S}_i$ is connected to the membrane unit $\mathcal{M}_i$. As shown in Fig. 3, each i-th spine unit $\mathcal{S}_i$ has registers storing the following discrete states.

Discrete LTP state

$$P_i \in \{0, 1, \cdots, P_{max}\},$$

Discrete LTD state

$$D_i \in \{0, 1, \cdots, D_{max}\},$$

where the integer parameters $P_{max} > 0$ and $D_{max} > 0$ determine the resolutions of the discrete LTP state P_i and the discrete LTD state D_i, respectively. As shown in Fig. 3, the spine $\mathcal{S}_i$ has the following internal clock.

Asynchronous internal clock for STDP

$$C_{Si}(t) = \begin{cases} 1 & \text{if } t \in \{t_{Si}^{(1)}, t_{Si}^{(2)}, \cdots\}, \\ 0 & \text{otherwise,} \end{cases}$$

where $t_{Si}^{(n)}$ represents spike timing (or rising edge) of the clock. In this paper, the internal clock C_{Si} is assumed to be periodic as shown in Fig. 6, to have different periods from the internal clocks C_{Vi}, C_{Ui}, and C_{Gi}, and to be asynchronous with C_{Vi}, C_{Ui}, and C_{Gi}. As shown in Fig. 6, the internal clock C_{Si}, the stimulation I_i, and the action potential Y_i trigger asynchronous transitions of the discrete states P_i and D_i of the spine unit $\mathcal{S}_i$ as follows.

Asynchronous transitions of LTP and LTD states

$$\begin{array}{ll} P_i(t^+) = P_{max} & \text{if } \ I_i(t) = 1, \\ P_i(t^+) = P_i(t) - 1 & \text{if } \ C_{Si}(t) = 1, \\ D_i(t^+) = D_{max} & \text{if } \ Y_i(t) = 1, \\ D_i(t^+) = D_i(t) - 1 & \text{if } \ C_{Si}(t) = 1. \end{array} \tag{7}$$

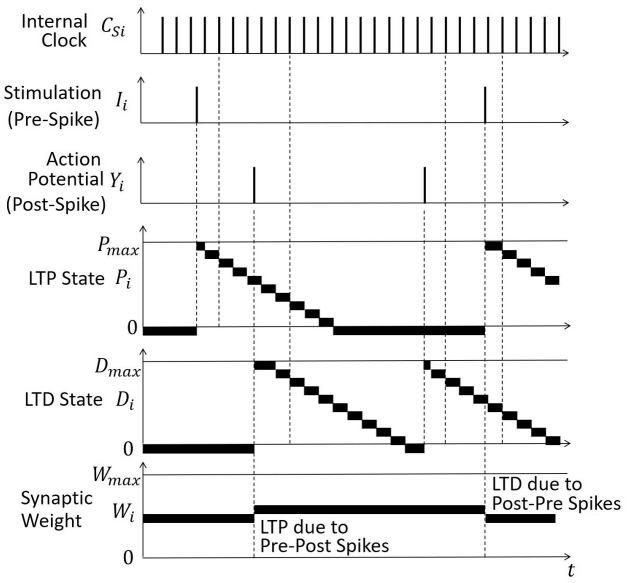

Fig. 6. Asynchronous discrete STDP of the spine unit $\mathcal{S}_i$.

Then, the stimulation I_i (i.e., pre-synaptic spike) to the spine unit $\mathcal{S}_i$ and the action potential Y_i (i.e., post-synaptic spike) from the membrane unit $\mathcal{M}_i$ trigger the following transitions of the synaptic weight W_i as shown in Fig. 6, where W_i is assumed to be saturated at 0 and W_{max} and to exist in its range $\{0, 1, \cdots, W_{max}\}$ throughout the paper.

Asynchronous discrete STDP

$$\begin{array}{ll} W_i(t^+) = W_i(t) + LTP(P_i(t)) & \text{if } Y_i(t) = 1, \\ W_i(t^+) = W_i(t) - LTD(D_i(t)) & \text{if } I_i(t) = 1, \end{array} \tag{8}$$

where $LTP : \{0, 1, \cdots, P_{max}\} \to \{0, 1\}$ and $LTD : \{0, 1, \cdots, D_{max}\} \to \{0, 1\}$ are discrete functions defined by

$$LTP(P) = \begin{cases} 0 & \text{if } P \leq 0, \\ 1 & \text{if } P > 0, \end{cases} \quad LTD(D) = \begin{cases} 0 & \text{if } D \leq 0, \\ 1 & \text{if } D > 0. \end{cases}$$

As shown in Fig. 6, the synaptic weight W_i is increased if an action potential $Y_i = 1$ (i.e., post-synaptic spike) comes to the spike unit $\mathcal{S}_i$ after a stimulation $I_i = 1$ (i.e., pre-synaptic spike) comes, and is decreased in the opposite case.

III. Analysis and design of multi-compartment soma-dendrite-spine model for STDP-based Pavlovian conditioning

A. Analysis of various propagations of action potentials

The multi-compartment soma-dendrite-spine model in Fig. 2 can exhibit a wide variety of propagations of action potentials, where some of typical ones are shown in Figs. 7-10. In these figures, the model receives the same stimulation I_4 from the spine unit $\mathcal{S}_4$, whereas the model has different values of the parameters α and β characterizing the coupling. Due to the differences of the parameter values, the model exhibits different propagations of action potentials as follows.

Type I propagation: In Fig. 7, the stimulation I_4 evokes rise of the membrane potential V_4 of the membrane unit $\mathcal{M}_4$ and generation of an action potential $Y_4 = 1$. Also, the rise of the membrane potential V_4 evokes rise of the membrane potential V_3 of the membrane unit $\mathcal{M}_3$ and generation of an action potential $Y_3 = 1$. In addition, these action potentials propagate to the soma compartment $\mathcal{M}_0$ and the soma compartment $\mathcal{M}_0$ generates an action potential $Y_0 = 1$. We refer to such a forward propagation of action potentials from spine to soma as a type I propagation.

Failure of type I propagation: In Fig. 8, the stimulation I_4 evokes rise of the membrane potential V_4 of the membrane unit $\mathcal{M}_4$ but the membrane unit $\mathcal{M}_3$ does not generate an action potential $Y_3 = 1$. We refer to such a phenomenon as failure of type I propagation.

Type II propagation: In Fig. 9, the stimulation I_4 evokes a forward propagation of action potentials but the propagation is not enough strong to make the soma compartment $\mathcal{M}_0$ fire. However, the rise of the membrane potential V_3 of the membrane unit $\mathcal{M}_3$ evokes rise of the membrane potential V_5 of the membrane unit $\mathcal{M}_5$ and generation of an action potential $Y_5 = 1$. We refer to such a backward propagation of action potentials from dendrite to spine evoked by the forward propagation as a type II propagation.

Type III propagation: In Fig. 10, the stimulation I_4 evokes a type I propagation, which evokes the following two backward propagations. (i) The rise of the membrane potential V_3 of the membrane unit $\mathcal{M}_3$ evokes rise of the membrane potential V_5 of the membrane unit $\mathcal{M}_5$ and generation of an action potential $Y_5 = 1$. (ii) The rise of the membrane potential V_0 and the action potential $Y_0 = 1$ of the soma compartment $\mathcal{M}_0$ evokes rise of the membrane potential V_1 of the membrane unit $\mathcal{M}_1$ and generation of an action potential $Y_1 = 1$. In addition, these action potentials propagate to the dendrite compartment $\mathcal{M}_5$ and then $\mathcal{M}_5$ generates an action potential $Y_5 = 1$. We refer to such of propagations of action potentials as a type III propagation.

Fig. 11 shows parameter regions in which the multi-compartment soma-dendrite-spine model exhibits the types I, II, and III propagations as follows.

Parameter region A: In the parameter region A, the model exhibits a type I propagation but does not exhibit a type II propagation or a type III propagation.

Parameter region B: In the parameter region B, the model does not exhibit a type I propagation, a type II propagation, or a type III propagation.

Parameter region C: In the parameter region C, the model exhibits a type II propagation but does not exhibit a type I propagation or a type III propagation.

Parameter region D: In the parameter region D, the model exhibits a type I propagation, a type II propagation, and a type III propagation.

The above analysis results are used as key tools to design the multi-compartment soma-dendrite-spine model to realize STDP-based Pavlovian conditioning.

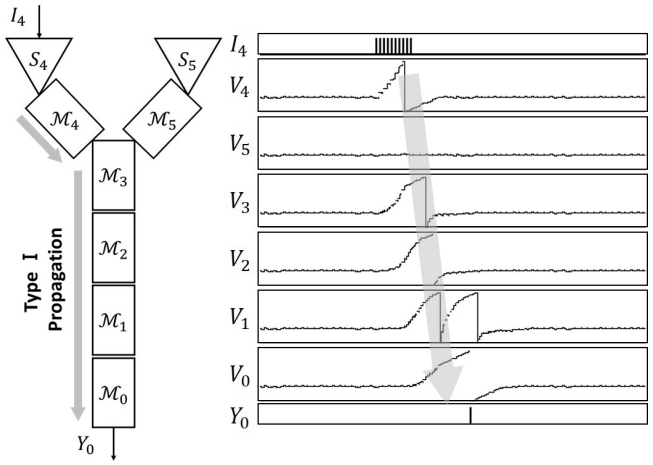

Fig. 7. Type I propagation. $(\alpha, \beta) = (0.35, 0.02)$ and $W_4 = 6$.

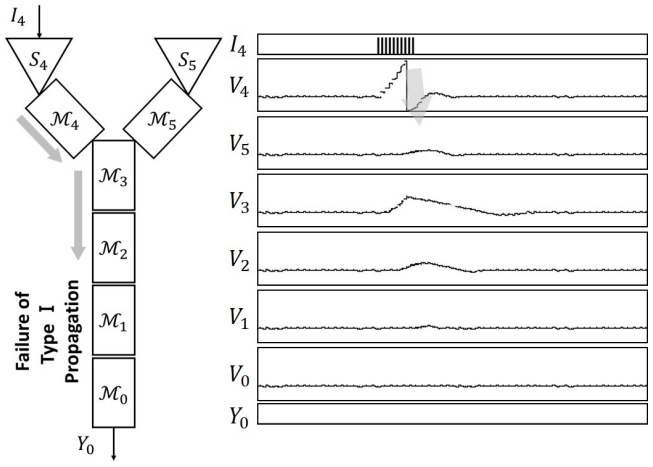

Fig. 8. Failure of Type I propagation. $(\alpha, \beta) = (0.16, 0.08)$ and $W_4 = 6$.

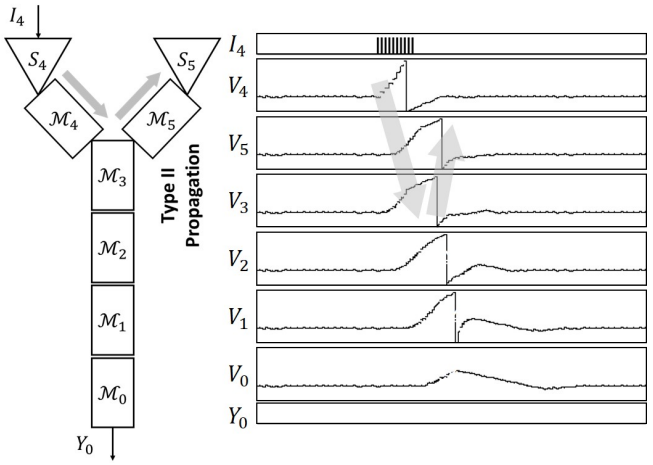

Fig. 9. Type II propagation. $(\alpha, \beta) = (0.19, 0.27)$ and $W_4 = 6$.

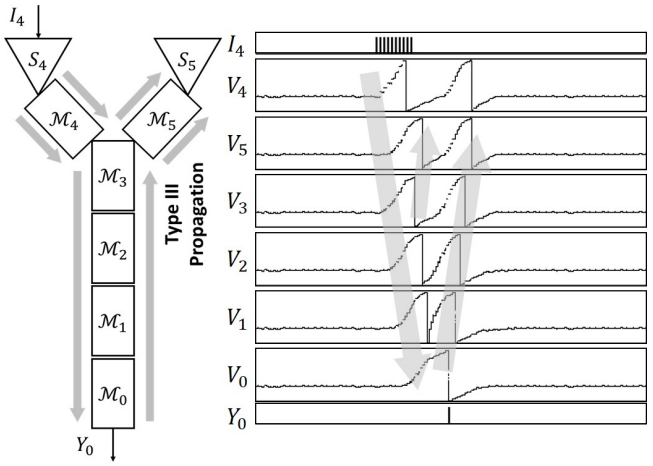

Fig. 10. Type III propagation. $(\alpha, \beta) = (0.4, 0.35)$ and $W_4 = 6$.

B. Design method for STDP-based Pavlovian conditioning

If the values of the parameters α and β are set in the parameter region D in Fig. 11, the spine unit $\mathcal{S}_5$ receives more action potentials Y_5 (i.e., more post-synaptic spikes) from the membrane unit $\mathcal{M}_5$ compared to the cases of the other parameter regions. Hence, the parameter region D is suited to realize conditioning or learning of the multi-compartment soma-dendrite-spine model based on the STDP. Then the following design method of the multi-compartment soma-dendrite-spine model to realize robust Pavlovian conditioning is proposed.

Design method for STDP-based Pavlovian conditioning

- Set the parameter values of each membrane unit $\mathcal{M}_i$ to $(M,\ N,\ f_1,\ f_2,\ f_3,\ f_4,\ f_5,\ B) = (64,\ 64,\ 3.5,\ 0.45,\ -0.05,\ 1.5,\ -0.43,\ 10)$ since this setting is suited to make the membrane unit $\mathcal{M}_i$ fireable.
- Set the parameter values of each spine unit $\mathcal{S}_i$ to $(P_{max}, D_{max}, W_{max}) = (500, 500, 6)$ since this setting is suited to cause action potentials of the membrane unit $\mathcal{M}_i$ for a wide range of stimulation I_i.
- Set the values of the parameters α and β in the parameter region D in Fig. 11 since this setting it suited to realize the STDP of the spine unit $\mathcal{M}_5$ for a wide range of stimulations I_4 and I_5.

Now, let us analyze Pavlovian conditioning of the multi-compartment soma-dendrite-spine model. Fig. 12 shows typical time waveforms of the model before the conditioning. In this case, the model salivates $Y_0 = 1$ in response to the food stimulation $I_4 = 1$ but does not for the bell stimulation $I_5 = 1$. Then the model is conditioned by giving the food stimulation $I_4 = 1$ and the bell stimulation $I_5 = 1$ repeatedly and randomly. Figs. 13-16 show typical time waveforms of the model after the conditioning. In Fig. 13, the model is designed by the proposed design method. In this case, the model salivates $Y_0 = 1$ in response to both the food stimulation $I_4 = 1$ and the bell stimulation $I_5 = 1$, and thus the model is properly conditioned. On the other hand, in Figs. 14, 15, and 16, the values of the parameters α and β are set in the parameter regions A, B, and C, respectively. In these cases, the model does not salivate $Y_0 = 1$ in response to the bell stimulation

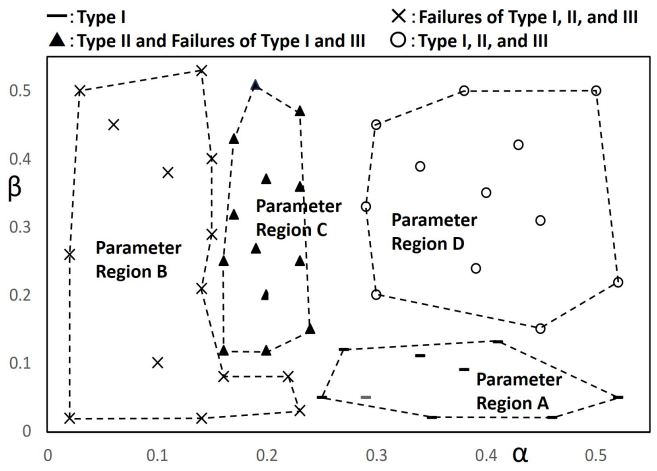

Fig. 11. Parameter regions of the propagations.

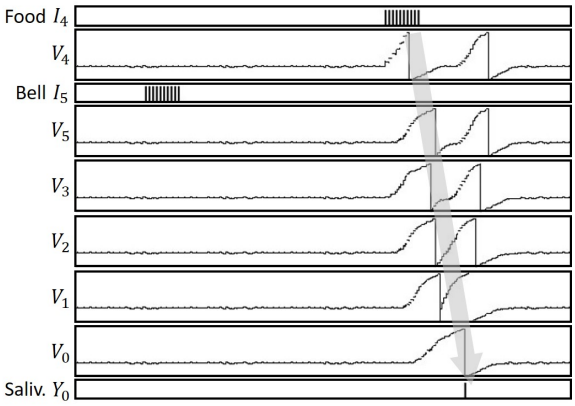

Fig. 12. Typical time waveforms of the model before STDP-based conditioning. $(W_4, W_5) = (6, 0)$. The model salivates for the food stimulation I_4 but does not salivate for the bell stimulation I_5.

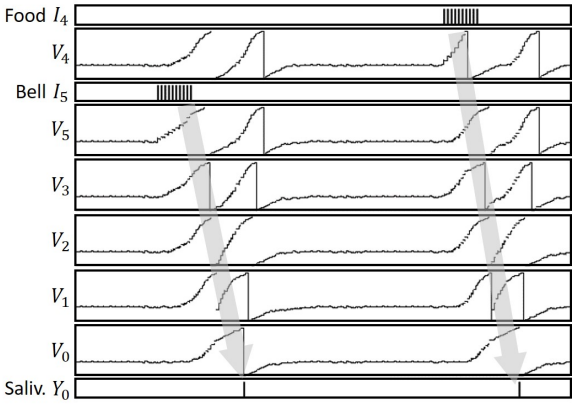

Fig. 13. Typical time waveforms of the model after STDP-based conditioning. The values of the parameters α and β are set in the parameter region D in Fig. 11. The model salivates for both the food stimulation I_4 and the bell stimulation I_5 and thus the model realizes the Pavlovian conditioning.

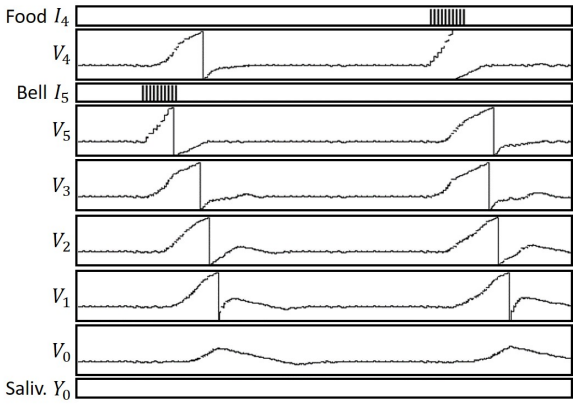

Fig. 14. Typical time waveforms of the model after STDP-based conditioning. The values of the parameters α and β are set in the parameter region C in Fig. 11. The model salivates only for the food stimulation I_4 and thus the model fails to realize the Pavlovian conditioning.

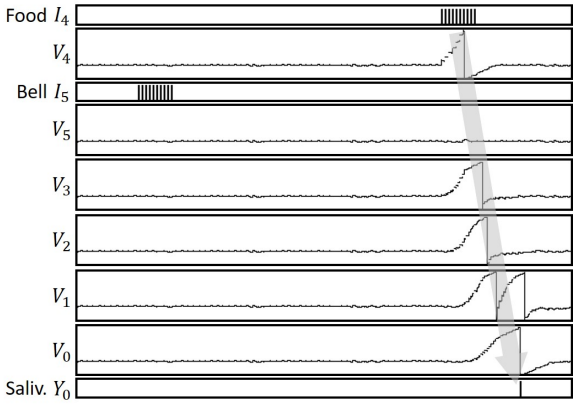

Fig. 15. Typical time waveforms of the model after STDP-based conditioning. The values of the parameters α and β are set in the parameter region A in Fig. 11. The model salivates only for the food stimulation I_4 and thus the model fails to realize the Pavlovian conditioning.

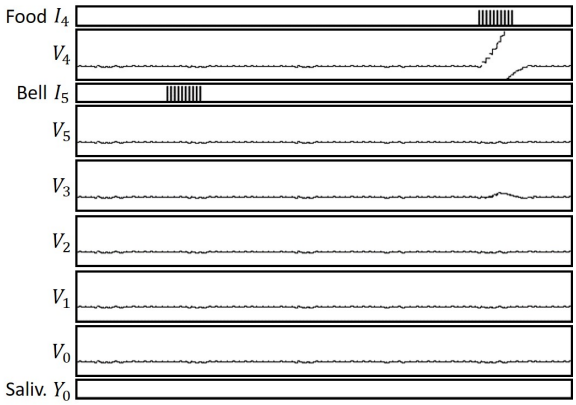

Fig. 16. Typical time waveforms of the model after STDP-based conditioning. The values of the parameters α and β are set in the parameter region B in Fig. 11. The model does not salivate and thus the model fails to realize the Pavlovian conditioning.

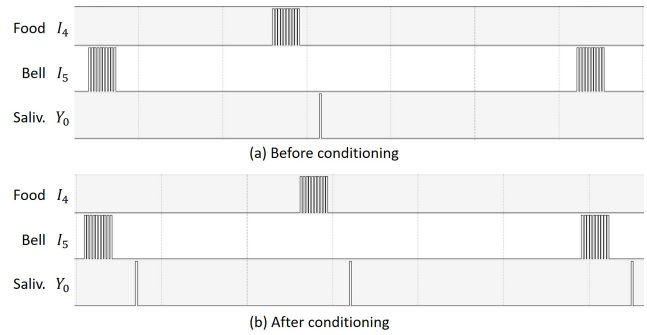

Fig. 17. Oscilloscope snapshots of FPGA-implemented multi-compartment soma-dendrite-spine model. (a) Before conditioning. (b) After conditioning.

$I_5 = 1$ and thus the model is not properly conditioned. So, it can be concluded that the proposed design method is useful to design the multi-compartment soma-dendrite-spine model capable of STDP-based conditioning.

IV. FPGA IMPLEMENTATION AND COMPARISONS

Recall that the dynamics of the multi-compartment soma-dendrite-spine model is described by Eqs. (1)-(8). These equations are rewritten as a register transfer level Verilog code. Then the code is compiled by Xilinx's design software environment Vivado Design Suite 2019.2.1 and the resulting bitstream file is implemented in Xilinx's *field programmable gate array* (FPGA) XC7Z020-1CLG484. Fig. 17 shows oscilloscope snapshots from the FPGA-implemented multi-compartment soma-dendrite-spine model designed by the proposed design method before and after the conditioning. It can be seen that the model salivates $Y_0 = 1$ in response to the food stimulation $I_4 = 1$ and the bell stimulation $I_5 = 1$ after the conditioning and thus the model is properly conditioned. For comparison, a multi-compartment soma-dendrite-spine model based on a numerical integration of the Izhikevich neuron model [9] is implemented by the same design software and in the same FPGA device. We confirmed that our model consumes much less hardware resources (about 1700 slices) and much less power (about 0.2 watt) compared to the model in [9] (about 4000 slices and about 0.5 watt).

V. CONCLUSIONS

It was shown that the multi-compartment soma-dendrite-spine model having the nonlinear dynamics of the asynchronous cellular automaton can exhibit various propagations of action potentials such as types I, II, and III propagations and their combinations. The intensive analyses revealed the parameter regions in which the model exhibits these propagations. Using the analysis results, the novel systematic design method of the model was proposed. It was shown that the proposed method is useful to design the model so that it can realize the robust STDP-based conditioning. In addition, we confirmed that the proposed method is effective for designing a multi-compartment model having more complex structure compared to that in this paper. It was also shown that the model designed by the proposed method consumes few hardware resources and low power. So, it can be concluded that the proposed design method will be a useful tool to design a biologically plausible neural network VLSI, whose applications include a biologically plausible neural prosthesis chip [19] such as a "*biologically plausible, small, low power, and robustly learnable brain implant chip.*"

REFERENCES

[1] The picture is from Wikimedia Commons. https://commons.wikimedia.org/wiki/File:Anatomy_of_a_Neuron_with_Synapse.png
[2] W. Rall, Electrophysiology of a Dendritic Neuron Model, Biophysical Journal, vol. 2, no. 2, pp. 145–167, 1962.
[3] G. Stuart, et al., Dendrites, 2nd Edition, Oxford University Press, 2007.
[4] I. Segev, J. Rinzel, and G. M. Shepherd, The Theoretical Foundation of Dendritic Function, The MIT Press, 2002.
[5] P. J. Sjostrom, et al., Dendritic Excitability and Synaptic Plasticity, Physiological Reviews, vol. 88, no. 2, pp. 769–840, 2008.
[6] I. Segev and M. London, Untangling dendrites with quantitative models, Science, vol. 290, no. 5492, pp. 744-750, 2000.
[7] W. R. Chen, J. Midtgaard, and G. M. Shepherd, Forward and Backward Propagation of Dendritic Impulses and Their Synaptic Control in Mitral cells, Science, vol. 278, no. 5337, pp. 463–467, 1997.
[8] E. Hay, S. Hill, F. Schurmann, H. Markram and I. Segev, Models of neocortical layer 5b pyramidal cells capturing a wide range of dendritic and perisomatic active properties, PLoS Computational Biology, vol. 7, no. 7, e1002107, 2011.
[9] E. M. Izhikevich, Dynamical Systems in Neuroscience, The MIT Press, 2010.
[10] C. Lammie, T. J. Hamilton, A. Schaik, and M. R. Azghadi, Efficient FPGA Implementations of Pair and Triplet-Based STDP for Neuromorphic Architectures, IEEE Trans. CAS-I vol. 66, no 4, pp. 1558-1570, 2019.
[11] N. Soures, L. Hays, E. Bohannon, A. M. Zyarah, and D. Kudithipudi, On-device STDP and synaptic normalization for neuromemristive spiking neural network, IEEE conf. 60th International MWSCAS, 2017.
[12] A. Shrestha, K. Ahmed, Y. Wang, and Q. Qiu, Stable spike-timing dependent plasticity rule for multilayer unsupervised and supervised learning, Proc. IJCNN, 2017.
[13] T. Naka and H. Torikai, A Novel Generalized Hardware-Efficient Neuron Model based on Asynchronous CA Dynamics and its Biologically Plausible On-FPGA Learnings, IEEE Trans. CAS-II vol. 66, no. 7, pp. 1247-1251, 2019.
[14] N. Shimada and H. Torikai, A novel Asynchronous Cellular Automaton Multi-Compartment Neuron Model, IEEE Trans. CAS-II, vol. 62, no. 8, pp. 776-780, 2015.
[15] K. Takeda and H. Torikai, A Novel Asynchronous CA Neuron Model: Design of Neuron-like Nonlinear Responses based on Novel Bifurcation Theory of Asynchronous Sequential Logic Circuit, IEEE Trans. CAS-I (accepted).
[16] A. Schmid, Neuromorphic microelectronics from devices to hardware systems and applications, NOLTA, IEICE, vol. 7, no. 4, pp. 468-498, 2016.
[17] K. Isobe and H. Torikai, A novel Hardware-Efficient Asynchronous Cellular Automaton Model of Spike-Timing Dependent Synaptic Plasticity, IEEE Trans. CAS-II, vol. 63, no. 6, pp. 603-607, 2016.
[18] K. Takeda and H. Torikai, A Novel Hardware-Efficient Cochlea Model based on Asynchronous Cellular Automaton Dynamics: Theoretical Analysis and FPGA Implementation, IEEE Trans. CAS-II, vol. 64, no. 9, pp. 1107–1111, 2017.
[19] T. Matsubara and H. Torikai, An Asynchronous Recurrent Network of Cellular Automaton-based Neurons and its Reproduction of Spiking Neural Network Activities, IEEE Trans. NNLS, vol. 27, no. 4, pp. 836-852, 2016.
[20] M. Gholami and S. Saeedi, Digital Cellular Implementation of Morris-Lecar Neuron, Proc. IEEE Iranian Conf. EE, pp. 1235-1239, 2015.
[21] S. G. Hu, et al., Synaptic long-term potentiation realized in Pavlov's dog model based on a NiOx-based memristor, J. of Applied Physics, vol. 116, no. 21, 214502, 2014.
[22] R. E. Hampon, *et al.*, Developing a Hippocampal Neural Prosthetic to Facilitate Human Memory Encoding and Recall, Journal of Neural Engineering, vol. 15, no. 3, 036014, 2018.